Two-mode Ginzburg-Landau theory of crystalline anisotropy for fcc-liquid interfaces

Kuo-An Wu* and Shang-Chun Lin
Department of Physics, National Tsing-Hua University, 30013 Hsinchu, Taiwan

Alain Karma
Physics Department and Center for Interdisciplinary Research on Complex Systems, Northeastern University, Boston, Massachusetts 02115, USA

(Received 24 December 2015; revised manuscript received 5 February 2016; published 24 February 2016)

We develop a Ginzburg-Landau (GL) theory for fcc crystal-melt systems at equilibrium by employing two sets of order parameters that correspond to amplitudes of density waves of principal reciprocal lattice vectors and amplitudes of density waves of a second set of reciprocal lattice vectors. The choice of the second set of reciprocal lattice vectors is constrained by the condition that this set must form closed triangles with the principal reciprocal lattice vectors in reciprocal space to make the fcc-liquid transition first order. The capillary anisotropy of fcc-liquid interfaces is investigated by GL theory with amplitudes of ⟨111⟩ and ⟨200⟩ density waves. Furthermore, we explore the dependence of the anisotropy of the excess free energy of the solid-liquid interface on density waves of higher-order reciprocal lattice vectors such as ⟨311⟩ by extending the two-mode GL theory with an additional mode. The anisotropy calculated using GL theory with input parameters from molecular dynamics (MD) simulations for fcc Ni is compared to that measured in MD simulations.

DOI: 10.1103/PhysRevB.93.054114

I. INTRODUCTION

The critical role of anisotropic interface properties on dendritic growth has been established in the past few decades analytically and numerically [1–6]. In particular, the anisotropy of the surface energy is one of the crucial physical quantities that controls the size and growth rates of dendrites under common solidification conditions where the solid-liquid interface can be assumed to be in local thermodynamic equilibrium. Several techniques have been developed to accurately compute the solid-liquid interfacial energy from molecular dynamics (MD) simulations and to successfully resolve its weak anisotropy [7–14]. In spite of its importance in metallurgy, it is of interest for scientists to understand the physical origin of the interfacial anisotropy. Recent studies have demonstrated that the small, yet important, interfacial anisotropy is related to the broken symmetry of the solid at the interface [15–17].

MD calculations for a wide range of systems show consistently that the capillary anisotropy for body-centered-cubic (bcc) elements is smaller than that for face-centered-cubic (fcc) ones [18,19]. Furthermore, the anisotropy parameters characterized by Kubic harmonics expansions have similar values for materials with the same crystal structures [11]. The universal observation that the interfacial anisotropy is closely related to crystal structures motivates the study of interfacial anisotropies using Ginzburg-Landau (GL) theory for bcc-liquid interfaces [15,20,21]. The order parameters of this theory are the amplitudes of density waves corresponding to the set of principal reciprocal lattice vectors, and the phenomenological coefficients in the GL theory are derived from density functional theory (DFT) of freezing [22–28]. The weak anisotropy of bcc-liquid systems calculated using the GL theory is in quantitatively good agreement with MD simulations [15]. Since the interfacial anisotropy is closely related to the lattice structure, the universality of the interfacial anisotropy for bcc-liquid systems is also derived in the phase field crystal (PFC) model [16,17,21] that is closely related to GL theory.

The PFC model introduced by Elder *et al.* has been successfully employed to tackle problems at the atomistic length scale over the past decade [29–46]. This model exhibits self-organized crystal-like structures, hence it is capable of describing crystalline planes, elastic and plastic deformations, and dislocations in crystals realistically. Thus, the PFC method is a powerful tool to model interfaces and microstructural evolution at atomistic scale due to its crystalline properties and above-mentioned structure-dependent interfacial anisotropy. However, in three dimensions, the stable crystal structure in the standard PFC model is the bcc lattice due to the fact that only wave vectors around the principal reciprocal lattice vectors in the PFC model are excited. Recent work has extended the PFC method to model other crystal structures of interest, such as fcc lattices [34,42], by incorporating more than one set of reciprocal lattice vectors. However, the resulting anisotropy of the solid-liquid interface free energy and its relationship to the choice reciprocal lattice vectors has not been analyzed in detail. In this paper, we employ the GL theory to investigate interfacial anisotropies for fcc crystals. In contrast to GL theory for bcc-liquid systems, the fourth-order GL theory with amplitudes of principal reciprocal lattice vectors cannot form stable fcc-liquid interfaces [47,48]. Thus, we consider the simplest fourth-order GL theory of the fcc-liquid interface with two sets of reciprocal lattice vectors. The formulation of two-mode GL theory is derived from density functional theory freezing using the set of ⟨200⟩ density waves as the second mode. The anisotropic density wave profiles and the anisotropy of interfacial energies are calculated. Furthermore, we examine the influence of higher-order reciprocal lattice vectors such as ⟨311⟩ on the anisotropy of the interfacial energy. The comparison of the anisotropy of the interfacial energy between GL theory and MD simulations is discussed.

*kuoan@phys.nthu.edu.tw

II. TWO-MODE GINZBURG-LANDAU THEORY

The GL theory of the bcc-liquid interfaces developed previously by Wu *et al.* successfully predicts the amplitude profiles and interfacial anisotropies [15]. The order parameters are the amplitudes of density waves corresponding to principal reciprocal lattice vectors $\langle 110\rangle$. The symmetries of principal reciprocal lattice vectors of bcc lattices result in nonvanishing cubic terms of amplitudes in the expansion of free energy in DFT of freezing. The cubic terms give rise to a free-energy barrier between the liquid and solid phases and make the bcc-liquid freezing transition first order [47]. However, for the fcc lattices, a single set of reciprocal lattice vectors alone cannot form a free-energy barrier due to the absence of the cubic term. Thus, to formulate a first-order solid-liquid phase transition for fcc lattices, one has to include not only the principal reciprocal lattice vectors $\langle 111\rangle$ but also a second set of reciprocal lattice vectors, which form closed triangles with $\langle 111\rangle$ in the reciprocal space. The candidates of the second mode are sets of the reciprocal lattice vectors that compose closed triads with $\langle 111\rangle$ in reciprocal space, such as $\langle 200\rangle, \langle 220\rangle$, etc. The number density of fcc lattices can be approximated by the following form:

$$n(\vec{r}) = n_0\left[1 + \sum_{\vec{K}_i} u_i(\vec{r}) e^{i\vec{K}_i\cdot\vec{r}} + \sum_{\vec{G}_i} v_i(\vec{r}) e^{i\vec{G}_i\cdot\vec{r}}\right], \quad (1)$$

where the order parameters u_i are amplitudes of density waves corresponding to principal reciprocal lattice vectors $\langle 111\rangle$ and v_i are amplitudes of density waves corresponding to the second set of reciprocal lattice vectors $\langle \vec{G}\rangle$. The free-energy functional in GL theory is derived from density functional theory of freezing; see Refs. [15,25,26]. The free-energy functional that describes small density fluctuations of an inhomogeneous liquid is

$$\Delta F = \frac{k_B T}{2}\iint d\vec{r}\, d\vec{r}\,' \delta n(\vec{r})\left[\frac{\delta(\vec{r}-\vec{r}\,')}{n_0} - C\big(|\vec{r}-\vec{r}\,'|\big)\right]\delta n(\vec{r}\,'), \quad (2)$$

where $\delta n(\vec{r}) \equiv n(\vec{r}) - n_0$, and $C(|\vec{r}-\vec{r}\,'|)$ is the two-particle direct correlation function of the liquid and with Fourier transform,

$$C(q) = n_0 \int d\vec{r}\, C(|\vec{r}|)\, e^{-i\vec{q}\cdot\vec{r}}, \quad (3)$$

is related to the liquid structure factor $S(q) = 1/[1 - C(q)]^{-1}$. Assuming a planar solid-liquid interface whose normal is along z direction and the amplitudes of density waves vary slowly across the interface, we can expand the density fluctuation $\delta n(\vec{r}\,')$ in a Taylor series about z,

$$\begin{aligned}\delta n\big(\vec{r}\,'\big) \approx n_0 \Bigg\{ &\sum_{\vec{K}_i}\left[u_i(z) + \frac{du_i(z)}{dz}(z'-z) + \frac{1}{2}\frac{d^2u_i(z)}{dz^2}(z'-z)^2\right]e^{i\,\vec{K}_i\cdot\vec{r}\,'} \\ &+ \sum_{\vec{G}_i}\left[v_i(z) + \frac{dv_i(z)}{dz}(z'-z) + \frac{1}{2}\frac{d^2v_i(z)}{dz^2}(z'-z)^2\right]e^{i\,\vec{G}_i\cdot\vec{r}\,'}\Bigg\}, \end{aligned} \quad (4)$$

where the higher-order terms are truncated under the assumption that the amplitudes u_i's and v_i's vary slowly across the interface. The excess free-energy functional is calculated by substituting this expression in Eq. (2) and carry out the integral over $\vec{r}\,'$.

In the integral over $\vec{r}\,'$, the contribution from terms that are independent of $(z - z')$ in Eq. (4) leads to

$$\begin{aligned} & n_0 \int d\vec{r}\,'\left[\frac{\delta(\vec{r}-\vec{r}\,')}{n_0} - C(|\vec{r}-\vec{r}\,'|)\right]\left[\sum_{\vec{K}_i} u_i(z) e^{i\vec{K}_i\cdot\vec{r}\,'} + \sum_{\vec{G}_i} v_i(z) e^{i\vec{G}_i\cdot\vec{r}\,'}\right], \\ &= \sum_{\vec{K}_i} u_i(z) e^{i\vec{K}_i\cdot\vec{r}}[1 - C(|\vec{K}_i|)] + \sum_{\vec{G}_i} v_i(z) e^{i\vec{G}_i\cdot\vec{r}}[1 - C(|\vec{G}_i|)] = \sum_{\vec{K}_i}\frac{1}{S(|\vec{K}_i|)} u_i(z) e^{i\vec{K}_i\cdot\vec{r}} + \sum_{\vec{G}_i}\frac{1}{S(|\vec{G}_i|)} v_i(z) e^{i\vec{G}_i\cdot\vec{r}}. \end{aligned} \quad (5)$$

The contribution from terms that are linearly proportional to $(z - z')$ in Eq. (4) is

$$\begin{aligned} & -n_0 \int d\vec{r}\,' C(|\vec{r}-\vec{r}\,'|)\left[\sum_{\vec{K}_i}\frac{du_i}{dz}(z'-z) e^{i\vec{K}_i\cdot\vec{r}\,'} + \sum_{\vec{G}_i}\frac{dv_i}{dz}(z'-z) e^{i\vec{G}_i\cdot\vec{r}\,'}\right], \\ &= \sum_{\vec{K}_i}\frac{du_i}{dz} e^{i\vec{K}_i\cdot\vec{r}}\left[i\,\frac{\partial C(|\vec{K}_i|)}{\partial K_z}\right] + \sum_{\vec{G}_i}\frac{dv_i}{dz} e^{i\vec{G}_i\cdot\vec{r}}\left[i\,\frac{\partial C(|\vec{G}_i|)}{\partial K_z}\right] \\ &= \sum_{\vec{K}_i}\frac{du_i}{dz} e^{i\vec{K}_i\cdot\vec{r}}[iC'(|\vec{K}_i|)(\hat{K}_i\cdot\hat{z})] + \sum_{\vec{G}_i}\frac{dv_i}{dz} e^{i\vec{G}_i\cdot\vec{r}}[iC'(|\vec{G}_i|)(\hat{G}_i\cdot\hat{z})], \end{aligned} \quad (6)$$

where $C'(q) \equiv dC(q)/dq$. It does not contribute to the integral over $\vec{r}$ in Eq. (2) since contribution from density wave of $+\vec{K}_i$ $(+\vec{G}_i)$ cancel with that of $-\vec{K}_i$ $(-\vec{G}_i)$. The contribution from terms that are proportional to $(z-z')^2$ in Eq. (4) is

$$
\begin{aligned}
&-\frac{n_0}{2}\int d\vec{r}\,' C(|\vec{r}-\vec{r}\,'|)\left[\sum_{\vec{K}_i}\frac{d^2u_i}{dz^2}(z'-z)^2 e^{i\vec{K}_i\cdot\vec{r}\,'}+\sum_{\vec{G}_i}\frac{d^2v_i}{dz^2}(z'-z)^2 e^{i\vec{G}_i\cdot\vec{r}\,'}\right],\\
&=\frac{1}{2}\sum_{\vec{K}_i}\frac{d^2u_i}{dz^2}e^{i\vec{K}_i\cdot\vec{r}}\left[\frac{\partial^2 C(|\vec{K}_i|)}{\partial K_z^2}\right]+\frac{1}{2}\sum_{\vec{G}_i}\frac{dv_i}{dz}e^{i\vec{G}_i\cdot\vec{r}}\left[\frac{\partial^2 C(|\vec{G}_i|)}{\partial K_z^2}\right]\\
&=\frac{1}{2}\sum_{\vec{K}_i}\frac{d^2u_i}{dz^2}e^{i\vec{K}_i\cdot\vec{r}}\left\{C''(|\vec{K}_i|)(\hat{K}_i\cdot\hat{z})^2+\frac{C'(|\vec{K}_i|)}{|\vec{K}_i|}\left[1-(\hat{K}_i\cdot\hat{z})^2\right]\right\}\\
&\quad+\frac{1}{2}\sum_{\vec{G}_i}\frac{d^2v_i}{dz^2}e^{i\vec{G}_i\cdot\vec{r}}\left\{C''(|\vec{G}_i|)(\hat{G}_i\cdot\hat{z})^2+\frac{C'(|\vec{G}_i|)}{|\vec{G}_i|}[1-(\hat{G}_i\cdot\hat{z})^2]\right\},
\end{aligned}
\tag{7}
$$

where $C''(q) \equiv d^2C(q)/dq^2$. Finally, the excess free-energy functional Eq. (2) is

$$
\begin{aligned}
\Delta F \approx \frac{n_0 k_B T}{2}\int d\vec{r}\Bigg(&\sum_{i,j}\frac{1}{S(|\vec{K}_i|)}u_i u_j\,\delta_{0,\vec{K}_i+\vec{K}_j}+\sum_{i,j}\frac{1}{S(|\vec{G}_i|)}v_i v_j\,\delta_{0,\vec{G}_i+\vec{G}_j}\\
&-\sum_i\frac{1}{2}\left\{C''(|\vec{K}_i|)(\hat{K}_i\cdot\hat{z})^2+\frac{C'(|\vec{K}_i|)}{|\vec{K}_i|}[1-(\hat{K}_i\cdot\hat{z})^2]\right\}\left|\frac{du_i}{dz}\right|^2\\
&-\sum_i\frac{1}{2}\left\{C''(|\vec{G}_i|)(\hat{G}_i\cdot\hat{z})^2+\frac{C'(|\vec{G}_i|)}{|\vec{G}_i|}[1-(\hat{G}_i\cdot\hat{z})^2]\right\}\left|\frac{dv_i}{dz}\right|^2\Bigg).
\end{aligned}
\tag{8}
$$

Since the magnitude of the principal reciprocal lattice vectors is determined by the location of the first peak of the liquid structure factor, the first derivative of $C(q)$ vanishes for $q = |\vec{K}|$. However, for the second set of reciprocal lattice vectors $\langle\vec{G}\rangle$, the coefficient of the square gradient terms depends on the details of the shape of $C(q)$ around $q = |\vec{G}|$ and also depends on the magnitude of the transverse component of the reciprocal lattice vectors. In order to have stable density wave profiles across solid-liquid interfaces, the coefficient of the square gradient terms must be positive, which requires both $C'(q) \leqslant 0$ and $C''(q) \leqslant 0$ for all reciprocal lattice vectors considered. To construct a simple two-mode GL theory for fcc-liquid systems, cubic and quartic terms of u and v are required. The symmetry of reciprocal lattice vectors determines which combination of polynomials of u_i's and v_i's is allowed in the GL free-energy functional as discussed in the following sections.

III. GL THEORY WITH ⟨111⟩ AND ⟨200⟩ MODES

The GL theory of equilibrium solid-liquid systems is derived from DFT of freezing as shown in the previous section, and the free energy is expanded as a power series of u_i's and v_i's around its liquid state. We first illustrate a simple GL theory for fcc-liquid systems by considering ⟨200⟩ reciprocal lattice vectors as the second mode. With ⟨111⟩ principal reciprocal lattice vectors and ⟨200⟩ reciprocal lattice vectors, the simplest form of the excess free energy of fcc-liquid systems can be written as

$$
\begin{aligned}
\Delta F \approx \frac{n_0 k_B T}{2}\int d\vec{r}\Bigg[&a_2\sum_{i,j}c_{ij}\,u_i u_j\,\delta_{0,\vec{K}_i+\vec{K}_j}+b_u\sum_i c_i\left|\frac{du_i}{dz}\right|^2+b_2\sum_{i,j}d_{ij}\,v_i v_j\,\delta_{0,\vec{G}_i+\vec{G}_j}+\sum_i\left(b_v^L d_i^L+b_v^T d_i^T\right)\left|\frac{dv_i}{dz}\right|^2\\
&-a_3\sum_{i,j,k}c_{ijk}\,u_i u_j v_k\,\delta_{0,\vec{K}_i+\vec{K}_j+\vec{G}_k}+a_4\sum_{i,j,k,l}c_{ijkl}\,u_i u_j u_k u_l\,\delta_{0,\vec{K}_i+\vec{K}_j+\vec{K}_k+\vec{K}_l}+b_4\sum_{i,j,k,l}d_{ijkl}\,u_i u_j v_k v_l\,\delta_{0,\vec{K}_i+\vec{K}_j+\vec{G}_k+\vec{G}_l}\Bigg],
\end{aligned}
\tag{9}
$$

where

$$
a_2 = \frac{8}{S(|\vec{K}_{111}|)}, \tag{10}
$$

$$
b_2 = \frac{6}{S(|\vec{G}_{200}|)}, \tag{11}
$$

$c_{ij} = 1/8$ and $d_{ij} = 1/6$. The interface normal is represented by $\hat{n}$ and it is set to be along the z direction. The coefficients of square gradient terms are

$$b_u c_i = -\frac{1}{2} C''(|\vec{K}_{111}|) \times (\hat{K}_i \cdot \hat{n})^2, \tag{12}$$

$$b_v^L d_i^L = -\frac{1}{2} C''(|\vec{G}_{200}|) \times (\hat{G}_i \cdot \hat{n})^2, \tag{13}$$

$$b_v^T d_i^T = -\frac{1}{2} \frac{C'(|\vec{G}_{200}|)}{|\vec{G}_{200}|} [1 - (\hat{G}_i \cdot \hat{n})^2], \tag{14}$$

where we divide the coefficient of the square gradient terms for $v_{\vec{G}}$'s into the longitudinal part, which depends on the value of the longitudinal component of $\hat{G}$, and the transverse part, which depends on the value of the transverse components of $\hat{G}$. Summing both sides of Eq. (12) and using the normalization $\sum_i c_i = 1$ gives

$$b_u = -\tfrac{4}{3} C''(|\vec{K}_{111}|), \tag{15}$$

and

$$c_i = \tfrac{3}{8} (\hat{K}_i \cdot \hat{n})^2. \tag{16}$$

Similarly, using the normalization $\sum_i d_i^L = 1$ and $\sum_i d_i^T = 1$ we obtain

$$b_v^L = -C''(|\vec{G}_{200}|), \tag{17}$$

$$d_i^L = \tfrac{1}{2} (\hat{G}_i \cdot \hat{n})^2. \tag{18}$$

$$b_v^T = -2 \frac{C'(|\vec{G}_{200}|)}{|\vec{G}_{200}|}, \tag{19}$$

$$d_i^T = \tfrac{1}{4} (1 - (\hat{G}_i \cdot \hat{n})^2). \tag{20}$$

It is clear that the nonvanishing cubic term is a result of closed triangles formed by two ⟨111⟩ vectors and one ⟨200⟩ vector in the reciprocal space (e.g., $[11\bar{1}]$,$[1\bar{1}1]$, and $[\bar{2}00]$ as shown in Fig. 1). In addition, two ⟨111⟩ vectors and two ⟨200⟩ vectors form closed four-side polygons in reciprocal space, which give rise to quartic terms $u_i u_j v_k v_l$ in the excess free energy. These quartic terms naturally ensure the stability of the solid state. The coefficients c_{ijk}, c_{ijkl}, and d_{ijkl} are determined by the ansatz that all geometrically distinct polygons in reciprocal space with the same number of sides have the same weight [15,20], and the sums of the c's and d's are normalized to unity, which yields $c_{ijk} = 1/12$, $c_{ijkl} = 1/12$, and $d_{ijkl} = 1/24$. Note that the equal-weight ansatz is made due to the lack of information of the higher-order direct correlation functions, which are difficult to obtain. Generally, the weight of polygons with n sides is related to the n-particle direct correlation function, which not only depends on the magnitude of reciprocal lattice vectors but also the angles between these vectors [49]. Different ansatz for the weight of polygons is discussed in the derivation of amplitude equations of PFC model [21] and also by Tóth and Provatas [17]. If one assumes higher-order correlation functions are constant, then all closed polygons (all repetitive closed polygons) have the same weight, which yields $c_{ijk} = 1/24$, $c_{ijkl} = 1/216$, and $d_{ijkl} = 1/96$. The multiplicative factors a_3, a_4, and b_4 are obtained by bulk properties at equilibrium as stated below. In bulk phases, amplitudes of the same set of reciprocal lattice vectors are equal (i.e., $u_i = u$ and $v_i = v$ for all i), which yields the excess free-energy functional of the bulk phases,

$$\Delta F \approx \frac{n_0 k_B T}{2} \int d\vec{r} (a_2 u^2 + b_2 v^2 - a_3 u^2 v + a_4 u^4 + b_4 u^2 v^2). \tag{21}$$

The coefficients a_3, a_4, and b_4 are determined by the constraints that the equilibrium state of the solid is a minimum of the free energy, $\partial \Delta F / \partial u|_{u=u_s} = 0$ and $\partial \Delta F / \partial v|_{v=v_s} = 0$, where u_s and v_s are the values of corresponding order parameters in the solid. And solid and liquid have equal free energy at the melting temperature, $\Delta F(u_s, v_s) = 0$. We obtain

$$\begin{aligned} a_3 &= 2\frac{a_2}{v_s} + 2\frac{b_2 v_s}{u_s^2}, \\ a_4 &= \frac{b_2 v_s^2}{u_s^4}, \\ b_4 &= \frac{a_2}{v_s^2}. \end{aligned} \tag{22}$$

Figure 2 shows a schematic plot for the excess free energy of the bulk phase as a function of the order parameter profiles u and v under the isotropic approximation (i.e., $u_i = u(z)$ and $v_i = v(z)$ for all i). The bulk free energy of the two-mode GL theory features a double well free energy as that in the GL theory for bcc-liquid systems at equilibrium. It is clear that the

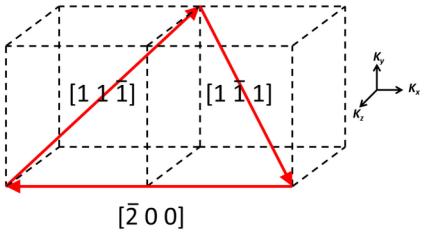

FIG. 1. Example of principal reciprocal lattice vectors of fcc lattices forming a closed triangle in reciprocal space.

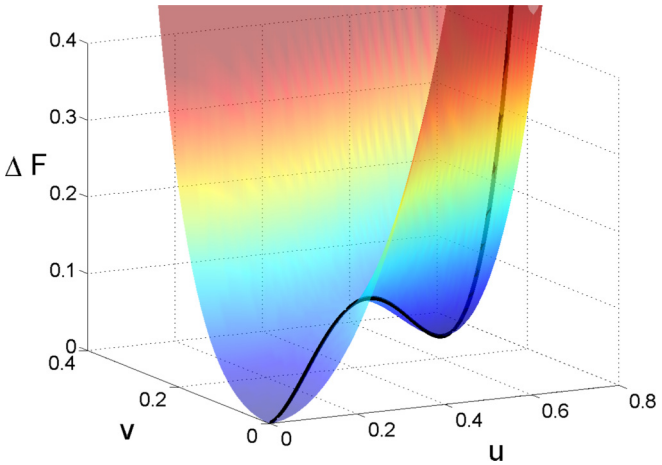

FIG. 2. Schematic plot of the excess free energy of GL theory for fcc lattices as a function of density waves amplitudes u and v under isotropic approximation.

TABLE I. List of symbols representing density waves used in GL calculation for the (100), (110), and (111) crystal faces.

	100			110				111		
Subset of	$\langle 111\rangle$	$\langle 200\rangle$	$\langle 200\rangle$	$\langle 111\rangle$	$\langle 111\rangle$	$\langle 200\rangle$	$\langle 200\rangle$	$\langle 111\rangle$	$\langle 111\rangle$	$\langle 200\rangle$
$(\hat{K}_i\cdot\hat{n})^2$ or $(\hat{G}_i\cdot\hat{n})^2$	1/3	1	0	2/3	0	1/2	0	1	1/9	1/3
Number of $\vec{K}_i$'s or $\vec{G}_i$'s	8	2	4	4	4	4	2	2	6	6
Order parameter	u_1	v_1	v_2	u_1	u_2	v_1	v_2	u_1	u_2	v_1

amplitudes of the density waves in the same set of reciprocal lattice vectors in the solid phase are the same and vanish in the liquid phase. However, the amplitudes of the density waves decay at various rates into the liquid phase, which gives rise to the interfacial anisotropies. It can be seen explicitly from the prefactors of the square gradient terms in Eq. (9). The prefactors are proportional to the square of the inner product of $\hat{K}_i$ (or $\hat{G}_i$) and the interface normal $\hat{n}$. To evaluate anisotropies of the interfacial free energy, we compute amplitude profiles and interfacial energies for the three low-index crystal faces (100), (110), and (111), respectively.

For (100) crystal faces, the eight principal reciprocal lattice vectors have the same symmetry with respect to the interface normal, which yield the same value of $(\hat{K}_i\cdot\hat{n})^2 = 1/3$, and the corresponding amplitudes are described by u_1. The second set of reciprocal lattice vectors can be divided into two subsets, which have the value of $(\hat{G}_i\cdot\hat{n})^2 = 1$ and 0, respectively, and the corresponding amplitudes are described by the order parameter v_1 and v_2. With these three order parameters, the excess free energy shown in Eq. (9) for (100) crystal faces reduces to

$$\Delta F_{100} = \frac{n_0 k_B T}{2}\int d\vec{r}\Big[a_2u_1^2 - \frac{a_3}{3}\big(u_1^2v_1 + 2u_1^2v_2\big) + a_4u_1^4 + \frac{b_2}{3}\big(v_1^2 + 2v_2^2\big) + \frac{b_4}{6}\big(u_1^2v_1^2 + 3u_1^2v_2^2 + 2u_1^2v_1v_2\big) + b_u\left|\frac{du_1}{dz}\right|^2 + b_v^L\left|\frac{dv_1}{dz}\right|^2 + b_v^T\left|\frac{dv_2}{dz}\right|^2\Big]. \tag{23}$$

Similarly, for (110) crystal faces, the set of principal reciprocal lattice vectors can be divided into two sets with amplitudes u_1 and u_2, and each set contains four reciprocal lattice vectors. Also the second set of the reciprocal lattice vectors can be divided into two sets having amplitudes v_1 and v_2, respectively. Subsets of density waves for (110) crystal faces are listed in Table I. For (110) crystal faces, we have

$$\Delta F_{110} = \frac{n_0 k_B T}{2}\int d\vec{r}\Big[\frac{a_2}{2}\big(u_1^2 + u_2^2\big) - \frac{a_3}{6}\big(u_1^2v_2 + u_2^2v_2 + 4u_1u_2v_1\big) + \frac{a_4}{4}\big(u_1^4 + u_2^4 + 2u_1^2u_2^2\big) + \frac{b_2}{3}\big(2v_1^2 + v_2^2\big) + \frac{b_4}{12}\big(3u_1^2v_1^2 + u_1^2v_2^2 + 3u_2^2v_1^2 + u_2^2v_2^2 + 4u_1u_2v_1v_2\big) + b_u\left|\frac{du_1}{dz}\right|^2 + \left(b_v^L + \frac{b_v^T}{2}\right)\left|\frac{dv_1}{dz}\right|^2 + \frac{b_v^T}{2}\left|\frac{dv_2}{dz}\right|^2\Big]. \tag{24}$$

For (111) crystal faces, the set of principal reciprocal lattice vectors can be divided into two sets while the second set of reciprocal lattice vectors has the same value of $(\hat{G}_i\cdot\hat{n})^2$ for all six vectors. The excess free energy for (111) crystal faces is

$$\Delta F_{111} = \frac{n_0 k_B T}{2}\int d\vec{r}\Big[\frac{a_2}{4}\big(u_1^2 + 3u_2^2\big) - \frac{a_3}{2}\big(u_2^2v_1 + u_1u_2v_1\big) + \frac{a_4}{12}\big(u_1^4 + 6u_2^4 + 3u_1^2u_2^2 + 2u_1u_2^3\big) + b_2v_1^2 + \frac{b_4}{8}\big(u_1^2v_1^2 + 5u_2^2v_1^2 + 2u_1u_2v_1^2\big) + \frac{b_u}{4}\left(3\left|\frac{du_1}{dz}\right|^2 + \left|\frac{du_2}{dz}\right|^2\right) + \big(b_v^L + b_v^T\big)\left|\frac{dv_1}{dz}\right|^2\Big]. \tag{25}$$

Subsets of density waves and their corresponding order parameters for each crystal faces are summarized in Table I.

The input parameters for the GL theory include the liquid structure factor and the values of order parameters in bulk solid. This information is obtained by MD simulations using the embedded-atom method (EAM) potential of Foiles, Baskes, and Daw (FBD) for Ni [50]; we obtain $S(|\vec{K}_{111}|) = 2.9898$, $S(|\vec{G}_{200}|) = 1.0162$, $C''(|\vec{K}_{111}|) = -9.1579\ \text{Å}^2$, $C'(|\vec{G}_{200}|) = -2.0303$ Å, and $C''(|\vec{G}_{200}|) = -0.0998\ \text{Å}^2$; see Fig. 3. The first peak of the liquid structure factor is located at $|K_{111}| = 3.0376\ \text{Å}^{-1}$. In order to obtain the magnitude of order parameters in solids, we assume that the density of atoms can be represented by a sum of Gaussian peaks centered at lattice sites $\vec{R}_i$, which leads to $n(\vec{r}) = \sum_i (\frac{1}{2\sigma^2\pi})^{3/2} e^{-(\vec{r}-\vec{R}_i)^2/2\sigma^2}$, where σ^2 is the variance of the Gaussian function. Under this assumption, the Fourier amplitudes of the density are simple functions of the magnitude of the corresponding wave number, $n(\vec{r}) = n_0(1 + \sum_i n_{\vec{K}_i} e^{i\vec{K}_i\cdot\vec{r}} + \sum_i n_{\vec{G}_i} e^{i\vec{G}_i\cdot\vec{r}} + \cdots)$, where $n_{\vec{K}_i} = e^{-\sigma^2K_i^2/2}$ and $n_{\vec{G}_i} = e^{-\sigma^2G_i^2/2}$. The variance σ^2 of the Gaussian function is estimated by the mean-square displacements of atoms in solids measured from MD simulations, $\sigma^2 = \frac{1}{3}\langle\Delta\vec{r}^2\rangle = 0.089\ \text{Å}^2$. Recognizing that the order parameters in

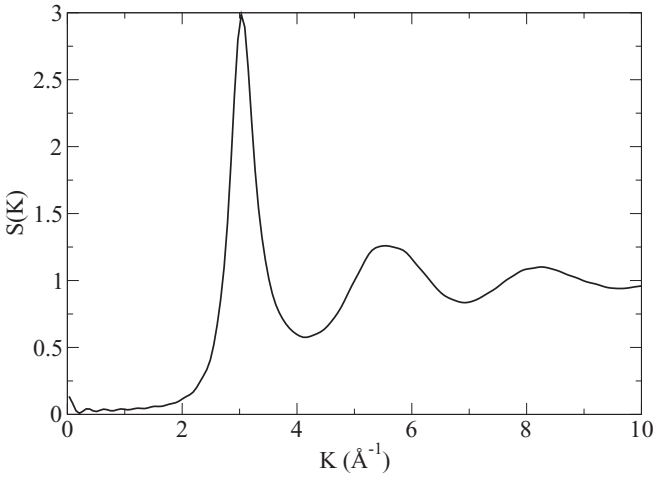

FIG. 3. The liquid structure factor of Ni at the melting temperature from MD simulations using EAM FBD potential.

bulk solids are the Fourier amplitudes of the density, we obtain

$$u_{111}(\text{solid}) = e^{-\sigma^2 K_{111}^2/2} = 0.6639,$$
$$v_{200}(\text{solid}) = e^{-\sigma^2 G_{200}^2/2} = 0.5791. \quad (26)$$

The values of input parameters from MD simulations are listed in Table II. With the above input parameters, the order parameter profiles for solid-liquid interfaces are solved by requiring that the free-energy functional is minimum with the corresponding order parameters profiles. The variational process leads to coupled Euler-Lagrange equations, which are solved numerically subject to the boundary conditions that these order parameters vanish in bulk liquids and retain fixed values in bulk solids shown in Eq. (26). The order parameters profiles for crystal faces (100), (110), and (111) are plotted in Figs. 4(a), 4(b), and 4(c), respectively.

The interfacial free energies are then computed with the equilibrium order parameter profiles solved above. In order to map out the anisotropy of the solid-liquid interfacial free energy, we employ the Kubic harmonics expansion for γ. The interfacial free energy $\gamma(\hat{n})$ can be parameterized by an expansion in terms of Kubic harmonics [51,52]. In terms of the Cartesian components of $\hat{n} = (n_x, n_y, n_z)$, the Kubic harmonic expansion for a weakly anisotropic crystal is [52]

$$\gamma(\hat{n}) = \gamma_0 \left[1 + \epsilon_1 \left(\sum_i n_i^4 - \frac{3}{5} \right) + \epsilon_2 \left(3 \sum_i n_i^4 + 66 n_x^2 n_y^2 n_z^2 - \frac{17}{7} \right) \right], \quad (27)$$

where γ_0 is the average interfacial free energy, and (ϵ_1, ϵ_2) characterize the capillary anisotropy. Note that for a more

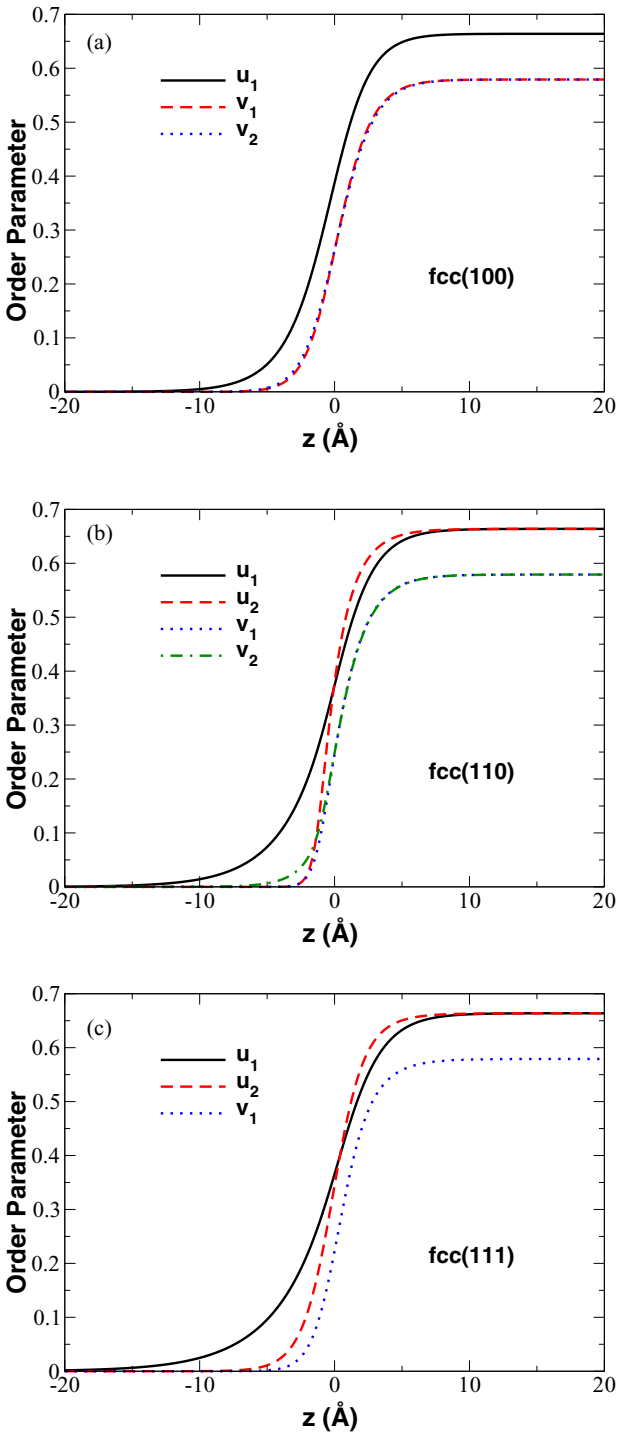

FIG. 4. Equilibrium density wave profiles across the solid-liquid interface obtained by GL theory with ⟨200⟩ mode with input parameters from MD simulations using EAM FBD potential of Ni for three low-index crystal orientations: (a) (100), (b) (110), and (c) (111).

TABLE II. Values of input parameters from MD simulations with interatomic EAM FBD potential for Ni [50] and resulting coefficients used in GL theory with ⟨200⟩ as the second mode.

	a_2	b_2	b_u (Å^2)	b_v^L (Å^2)	b_v^T (Å^2)	u_s	v_s	$\lvert\vec{K}_i\rvert$ (Å^{-1})	$\lvert\vec{G}_i\rvert$ (Å^{-1})
MD [FBD]	2.68	5.90	12.21	0.07	1.16	0.66	0.58	3.0376	3.5075

TABLE III. Anisotropy parameters for the fcc-liquid interfacial free energy predicted by the present GL theory with ⟨200⟩ mode that assumes equal weights of geometrically distinct polygons, the GL theory with ⟨200⟩ mode that assumes equal weights of all polygons [17,21], the present GL theory with ⟨200⟩ and ⟨311⟩ modes that assumes equal weights of geometrically distinct polygons, and MD simulations [11].

	ϵ_1	ϵ_2	$(\gamma_{100}-\gamma_{110})/2\gamma_0$	$(\gamma_{100}-\gamma_{111})/2\gamma_0$
GL theory with ⟨200⟩ mode	0.1084	0.0157	0.0389	0.0329
GL theory with ⟨200⟩ mode (Refs. [17,21])	0.1221	0.0191	0.0448	0.0368
GL theory with ⟨200⟩ and ⟨311⟩ modes	0.1038	0.0149	0.0371	0.0315
MD Ni (FBD) (Ref. [11])	0.088(7)	−0.011(1)	0.014(2)	0.032(2)

anisotropic crystal, higher-order Kubic harmonics are necessary to characterize the interfacial anisotropy [53]. With solid-liquid interfacial free energies γ_{100}, γ_{110}, and γ_{111} obtained above, we find $\gamma_0 = 106.22$ erg/cm^2, $\epsilon_1 = 0.1084$, and $\epsilon_2 = 0.0157$, see Table III. The average interfacial free energy estimated by GL theory is lower than that measured in MD simulation, $\gamma_{\rm MD} = 284.7$ erg/cm^2, since the two-mode GL theory truncates contributions of higher-order density waves and it assumes a weak first-order phase transition. Nevertheless, the two-mode GL theory sheds light on the relation between interfacial anisotropy and crystal structure. The simple GL theory of fcc-liquid interface considering reciprocal lattice vectors ⟨111⟩ and ⟨200⟩ predicts reasonable magnitudes of ϵ_1 and ϵ_2 as compared to MD simulations [11]. However, the value of ϵ_2 obtained in GL theory has an opposite sign from that in MD simulations. It also gives different ordering of γ observed in MD simulations ($\gamma_{100} > \gamma_{110} > \gamma_{111}$) and in GL theory ($\gamma_{100} > \gamma_{111} > \gamma_{110}$). Similar results are obtained for the GL theory using different equal-weight polygon ansatz [17,21], $\epsilon_1 = 0.1221$, and $\epsilon_2 = 0.0191$; see Table III. The discrepancy between MD simulations and GL theory for fcc materials is likely due to the choice of the second mode. Even though ⟨200⟩ density waves form closed triangles with ⟨111⟩ density waves in reciprocal space, the amplitudes of ⟨200⟩ density waves in liquids at the melting temperature are not pronounced; see Fig. 3. Possible candidates of the second mode for GL theory are the density waves whose magnitude of the corresponding reciprocal lattice vectors is close to the position of the second peak of the liquid structure factor. The density waves that form closed triangles with ⟨111⟩ density waves and with the magnitude of reciprocal lattice vectors comparable to the position of the second peak of the liquid structure factor are ⟨220⟩ and ⟨222⟩ density waves. However, GL theory with the lowest-order expansion of gradient terms requires both $C'(q)$ and $C''(q)$ to be less than or equal to zero for all density waves considered in order to have stable density wave profiles. Thus, ⟨220⟩ and ⟨222⟩ density waves are excluded since $C'(|\vec{G}_{220}|) > 0$ and $C''(|\vec{G}_{222}|) > 0$; see Fig. 3.

IV. GL THEORY WITH ⟨111⟩, ⟨200⟩, AND ⟨311⟩ MODES

The density waves with the magnitude of the corresponding reciprocal lattice vectors close to the location of the second peak of the liquid structure factor are ⟨310⟩ and ⟨311⟩ density waves. Furthermore, since the ⟨311⟩ density waves form closed triangles with ⟨111⟩ and ⟨200⟩ density waves, we extend previous two-mode GL theory with an additional ⟨311⟩ mode to carry out the interfacial anisotropy calculations. The excess free-energy functional of GL theory that employs an additional ⟨311⟩ mode differs from that of GL theory discussed in previous section in the following additional terms,

$$\Delta F = \Delta F_{200} + \frac{n_0 k_B T}{2}\int d\vec{r}\left[d_2\sum_{i,j} e_{ij}\, w_i w_j\, \delta_{0,\vec{G}'_i+\vec{G}'_j} + \sum_i \left(b_w^L e_i^L + b_w^T e_i^T\right)\left|\frac{dw_i}{dz}\right|^2 - d_3\sum_{i,j,k} e_{ijk}\, u_i v_j w_k\, \delta_{0,\vec{K}_i+\vec{G}_j+\vec{G}'_k}\right], \quad (28)$$

where ΔF_{200} is the excess free-energy functional of GL theory employing merely ⟨111⟩ and ⟨200⟩ modes shown in Eq. (9); the set of reciprocal lattice vectors ⟨311⟩ is represented by $\langle G'\rangle$. Comparing it with Eq. (8), we obtain

$$d_2 = \frac{24}{S(|\vec{G}_{311}|)}, \quad (29)$$

$$e_{ij} = \frac{1}{24}, \quad (30)$$

$$b_w^L = -4C''(|\vec{G}_{311}|), \quad (31)$$

$$e_i^L = \frac{1}{8}(\hat{G}_i\cdot\hat{n})^2, \quad (32)$$

$$b_w^T = -8\frac{C'(|\vec{G}_{311}|)}{|\vec{G}_{311}|}, \quad (33)$$

$$e_i^T = \frac{1}{16}\left[1-(\hat{G}_i\cdot\hat{n})^2\right]. \quad (34)$$

The multiplicative factors a_3, d_3, a_4, and b_4 are obtained using equilibrium conditions as discussed before. The free energy of the bulk phase is

$$\Delta F \approx \frac{n_0 k_B T}{2}\int d\vec{r}(a_2 u^2 + b_2 v^2 - a_3 u^2 v + a_4 u^4 + b_4 u^2 v^2 - d_3 uvw + d_2 w^2). \quad (35)$$

By requiring $\partial\Delta F/\partial u|_{u=u_s} = 0$, $\partial\Delta F/\partial v|_{v=v_s} = 0$, $\partial\Delta F/\partial w|_{w=w_s} = 0$, and that solid and liquid have equal free energy at the melting temperature, $\Delta F(u_s, v_s, w_s) = 0$, we obtain

$$a_3 = 2\frac{a_2}{v_s} + 2\frac{b_2 v_s}{u_s^2}, \quad a_4 = \frac{b_2 v_s^2}{u_s^4}, \quad b_4 = \frac{a_2}{v_s^2} + \frac{d_2 w_s^2}{u_s^2 v_s^2}, \quad d_3 = 2\frac{d_2 w_s}{u_s v_s}. \quad (36)$$

TABLE IV. List of symbols representing ⟨311⟩ density waves used in GL calculation for (100), (110), and (111) crystal faces.

	100			110			111		
Subset of	⟨311⟩	⟨311⟩	⟨311⟩	⟨311⟩	⟨311⟩	⟨311⟩	⟨311⟩	⟨311⟩	⟨311⟩
$(\hat{G}_i' \cdot \hat{n})^2$	9/11	1/11	8/11	2/11	2/11	0	25/33	9/33	1/33
Number of $\vec{G}_i'$s	8	16	8	8	4	4	6	12	6
Order parameter	w_1	w_2	w_1	w_2	w_3	w_4	w_1	w_2	w_3

The normalization constant for the coupling term uvw is determined using the equal-weight ansatz for geometrically distinct polygons in reciprocal space that yields $e_{ijk} = 1/24$. For different crystal faces, we divide ⟨311⟩ density waves into several subsets according to values of direction cosines as listed in Table IV. Then the free-energy functionals for three crystal faces (100), (110), and (111) are

$$\Delta F_{100} = \frac{n_0 k_B T}{2} \int d\vec{r} \Big[a_2 u_1^2 - \frac{a_3}{3}\left(u_1^2 v_1 + 2u_1^2 v_2\right) + a_4 u_1^4 + \frac{b_2}{3}\left(v_1^2 + 2v_2^2\right) + \frac{b_4}{6}\left(u_1^2 v_1^2 + 3u_1^2 v_2^2 + 2u_1^2 v_1 v_2\right) + \frac{d_2}{3}\left(w_1^2 + 2w_2^2\right) - \frac{d_3}{3}(u_1 v_1 w_1 + 2u_1 v_2 w_2) + b_u \left|\frac{du_1}{dz}\right|^2 + b_v^L \left|\frac{dv_1}{dz}\right|^2 + b_v^T \left|\frac{dv_2}{dz}\right|^2 + \frac{b_w^L}{11}\left(9\left|\frac{dw_1}{dz}\right|^2 + 2\left|\frac{dw_2}{dz}\right|^2\right) + \frac{b_w^T}{11}\left(\left|\frac{dw_1}{dz}\right|^2 + 10\left|\frac{dw_2}{dz}\right|^2\right)\Big]. \tag{37}$$

$$\Delta F_{110} = \frac{n_0 k_B T}{2} \int d\vec{r} \Big[\frac{a_2}{2}\left(u_1^2 + u_2^2\right) - \frac{a_3}{6}\left(u_1^2 v_2 + u_2^2 v_2 + 4u_1 u_2 v_1\right) + \frac{a_4}{4}\left(u_1^4 + u_2^4 + 2u_1^2 u_2^2\right) + \frac{b_2}{3}\left(2v_1^2 + v_2^2\right) + \frac{b_4}{12}\left(3u_1^2 v_1^2 + u_1^2 v_2^2 + 3u_2^2 v_1^2 + u_2^2 v_2^2 + 4u_1 u_2 v_1 v_2\right) + \frac{d_2}{6}\left(2w_1^2 + 2w_2^2 + w_3^2 + w_4^2\right) - \frac{d_3}{6}(2u_1 v_1 w_1 + u_1 v_2 w_3 + 2u_2 v_1 w_2 + u_2 v_2 w_4) + b_u \left|\frac{du_1}{dz}\right|^2 + b_v^L \left|\frac{dv_1}{dz}\right|^2 + \frac{b_v^T}{2}\left(\left|\frac{dv_1}{dz}\right|^2 + \left|\frac{dv_2}{dz}\right|^2\right) + \frac{b_w^L}{11}\left(8\left|\frac{dw_1}{dz}\right|^2 + 2\left|\frac{dw_2}{dz}\right|^2 + \left|\frac{dw_3}{dz}\right|^2\right) + \frac{b_w^T}{44}\left(6\left|\frac{dw_1}{dz}\right|^2 + 18\left|\frac{dw_2}{dz}\right|^2 + 9\left|\frac{dw_3}{dz}\right|^2 + 11\left|\frac{dw_4}{dz}\right|^2\right)\Big]. \tag{38}$$

$$\Delta F_{111} = \frac{n_0 k_B T}{2} \int d\vec{r} \Big[\frac{a_2}{4}\left(u_1^2 + 3u_2^2\right) - \frac{a_3}{2}\left(u_2^2 v_1 + u_1 u_2 v_1\right) + \frac{a_4}{12}\left(u_1^4 + 6u_2^4 + 3u_1^2 u_2^2 + 2u_1 u_2^3\right) + b_2 v_1^2 + \frac{b_4}{8}\left(u_1^2 v_1^2 + 5u_2^2 v_1^2 + 2u_1 u_2 v_1^2\right) + \frac{d_2}{4}\left(w_1^2 + 2w_2^2 + w_3^2\right) - \frac{d_3}{4}(u_1 v_1 w_1 + 2u_2 v_1 w_2 + u_2 v_1 w_3) + \frac{b_u}{4}\left(3\left|\frac{du_1}{dz}\right|^2 + \left|\frac{du_2}{dz}\right|^2\right) + \left(b_v^L + b_v^T\right)\left|\frac{dv_1}{dz}\right|^2 + \frac{b_w^L}{44}\left(25\left|\frac{dw_1}{dz}\right|^2 + 18\left|\frac{dw_2}{dz}\right|^2 + \left|\frac{dw_3}{dz}\right|^2\right) + \frac{b_w^T}{44}\left(4\left|\frac{dw_1}{dz}\right|^2 + 24\left|\frac{dw_2}{dz}\right|^2 + 16\left|\frac{dw_3}{dz}\right|^2\right)\Big]. \tag{39}$$

The solid amplitude for ⟨311⟩ density waves is estimated to be 0.22 using the approximation of Gaussian density peaks. The values of input parameters from MD simulations are listed in Table V. The interfacial energies calculated for these three crystal faces yield $\gamma_0 = 109.37$ erg/cm^2, $\epsilon_1 = 0.1038$, and $\epsilon_2 = 0.0149$, see Table III. The additional ⟨311⟩ leads to a slightly larger magnitude of γ and predicts similar anisotropy parameters predicted by the two-mode GL theory.

TABLE V. Values of input parameters from MD simulations with interatomic EAM FBD potential for Ni [50] and resulting coefficients used in GL theory with ⟨311⟩ as the second mode.

	d_2	b_w^L (Å^2)	b_w^T (Å^2)	w_s	$\lvert\vec{G}_i\rvert$ (Å^{-1})
MD [FBD]	19.46	5.00	0.16	0.22	5.8166

V. DISCUSSION AND CONCLUSION

The simple two-mode GL theory shown above is capable of describing the interfacial anisotropies of fcc-liquid systems. However, the magnitude of the interfacial energy is about $2 \sim 3$ times smaller than predicted by MD simulations, and other physical quantities such as latent heat of fusion are also underestimated. Shih *et al.* relates the latent heat of fusion (per atom) to the temperature variation of the inverse of the peak of the liquid structure factor [20],

$$L = \frac{T_m}{N}\frac{\partial \Delta F}{\partial T}\bigg|_{T=T_m} = \frac{k_B T_m^2}{2} u_s^2 \frac{da_2}{dT}\bigg|_{T=T_m}, \tag{40}$$

where N is the number of atoms in the system. With parameters listed in Table II, Eq. (40) yields a latent heat value $L = 0.103$ eV/atom about 40% lower than the MD value ($L_{\mathrm{MD}} = 0.179$ eV/atom). The underestimation of the latent heat of fusion can be attributed to the truncation of the contribution of higher-order reciprocal lattice vectors in GL theory. In order to construct a GL theory with a limited number of modes that describes correct anisotropy of the interfacial energy and the latent heat of fusion, we can use Eq. (40) and the latent heat of fusion measured from MD simulations to set the magnitude of u_s, which yields $u_s = 0.87$. With this new input of solid amplitudes, the anisotropy of the interfacial energy remains the same while the magnitude of the interfacial energy increases linearly with the solid amplitude square as discussed below. For simplicity, assuming that density waves of the same set of reciprocal lattice vectors remain equal across the interface (i.e., isotropic approximation) and substituting Eq. (22) into Eq. (9), we obtain

$$\Delta F = \frac{n_0 k_B T}{2} u_s^2 \int d\vec{r}\Big[a_2 U^2(-1+V)^2 + b_2(U^2-V)^2\alpha^2 + b_u\left|\frac{dU}{dz}\right|^2 + \left(b_v^L + b_v^T\right)\alpha^2\left|\frac{dV}{dz}\right|^2\Big], \tag{41}$$

where we define $U \equiv (u/u_s)$, $V \equiv (v/v_s)$, and $\alpha = (v_s/u_s)$. The value of α is set by the Gaussian approximation of density peaks in solids. It is clear that the magnitude of the interfacial free energy is proportional to the square of the solid amplitude u_s^2. Similar arguments can be applied to anisotropic calculations; the square of the solid amplitude only affects the magnitude of γ. With u_s estimated by the latent heat of fusion, $u_s = 0.87$, we obtain $\gamma_{100} = 194.22$ erg/cm^2, $\gamma_{110} = 179.87$ erg/cm^2, and $\gamma_{111} = 182.08$ erg/cm^2.

We have formulated the simplest fourth-order GL theory of the fcc-liquid systems using two sets of amplitudes corresponding to principal reciprocal lattice vectors $\langle 111\rangle$ and a second set of reciprocal lattice vectors. The requirement for the second set of reciprocal lattice vectors is that it can form closed triangles with the principal reciprocal lattice vectors in reciprocal space, which ensures nonvanishing cubic terms in the GL free-energy functional, which makes the fcc-liquid transition first order. The phenomenological GL theory is derived from density functional theory of freezing, which ensures correct spatial decay rates of density waves that are related to the liquid structure factor. The crystalline anisotropy of interfacial energies is investigated with $\langle 111\rangle$ and $\langle 200\rangle$ density waves. The two-mode GL theory is shown to form stable fcc-liquid interfaces, and it predicts a weak anisotropy with $\langle 200\rangle$ mode. However, the cubic anisotropy parameter ϵ_2 calculated using $\langle 200\rangle$ mode has an opposite sign compared to that in MD simulations. Similar results are obtained by GL theory with different nonlinear coefficients (different ansatz of counting polygons), which suggests differences in nonlinear coefficients only have a small effect on the interfacial anisotropy. We extended the two-mode GL theory with an additional $\langle 311\rangle$ mode to explore the dependence of the interfacial anisotropy on higher order reciprocal lattice vectors. GL theory with an additional $\langle 311\rangle$ mode predicts similar anisotropy parameters as shown in two-mode GL theory. This suggests the third mode has a small effect on the interfacial anisotropy. These results are relevant to atomistic modeling of microstructural evolution [34,42], where the anisotropy of interfacial free-energies can be tuned by the second set of reciprocal lattice vectors and the shape of the liquid structure factor accordingly. An interesting future prospect is to extend the two-mode GL theory to investigate the anisotropy of kinetic coefficients based on recent progress for bcc ordering Ginzburg-Landau theory [54].

ACKNOWLEDGMENTS

We gratefully acknowledge the support of the National Science Council of Taiwan (Grant No. NSC102-2112-M-007-007-MY3), and the support from National Center for Theoretical Sciences, Taiwan. A.K. was supported by Grant No. DE-FG02-07ER46400 from the U.S. Department of Energy, Office of Basic Energy Sciences.

[1] D. A. Kessler, J. Koplik, and H. Levine, Adv. Phys. **37**, 255 (1988).
[2] M. Ben Amar and E. Brener, Phys. Rev. Lett. **71**, 589 (1993).
[3] A. Karma and W.-J. Rappel, Phys. Rev. Lett. **77**, 4050 (1996).
[4] A. Karma and W.-J. Rappel, Phys. Rev. E **57**, 4323 (1998).
[5] N. Provatas, N. Goldenfeld, and J. Dantzig, Phys. Rev. Lett. **80**, 3308 (1998).
[6] J. Hoyt, M. Asta, T. Haxhimali, A. Karma, R. Napolitano, R. Trivedi, B. B. Laird, and J. R. Morris, MRS Bull. **29**, 935 (2004).
[7] J. Q. Broughton and G. H. Gilmer, J. Chem. Phys. **84** (1986).
[8] R. L. Davidchack and B. B. Laird, Phys. Rev. Lett. **85**, 4751 (2000).
[9] J. J. Hoyt, M. Asta, and A. Karma, Phys. Rev. Lett. **86**, 5530 (2001).
[10] J. J. Hoyt and M. Asta, Phys. Rev. B **65**, 214106 (2002).
[11] J. Hoyt, M. Asta, and A. Karma, Mater. Sci. Eng. Rep. **41**, 121 (2003).
[12] R. L. Davidchack and B. B. Laird, J. Chem. Phys. **118**, 7651 (2003).
[13] R. L. Davidchack and B. B. Laird, Phys. Rev. Lett. **94**, 086102 (2005).
[14] R. L. Davidchack, J. R. Morris, and B. B. Laird, J. Chem. Phys. **125**, 094710 (2006).
[15] K.-A. Wu, A. Karma, J. J. Hoyt, and M. Asta, Phys. Rev. B **73**, 094101 (2006).
[16] A. Jaatinen, C. V. Achim, K. R. Elder, and T. Ala-Nissila, Phys. Rev. E **80**, 031602 (2009).
[17] G. I. Tóth and N. Provatas, Phys. Rev. B **90**, 104101 (2014).
[18] D. Y. Sun, M. Asta, J. J. Hoyt, M. I. Mendelev, and D. J. Srolovitz, Phys. Rev. B **69**, 020102 (2004).
[19] D. Y. Sun, M. Asta, and J. J. Hoyt, Phys. Rev. B **69**, 174103 (2004).
[20] W. H. Shih, Z. Q. Wang, X. C. Zeng, and D. Stroud, Phys. Rev. A **35**, 2611 (1987).

[21] K.-A. Wu and A. Karma, Phys. Rev. B **76**, 184107 (2007).
[22] J. K. Percus, in *The Equilibrium Theory of Classical Fluids*, edited by H. L. Frisch and J. L. Lebowitz (Benjamin, New York, 1964).
[23] R. Evans, Adv. Phys. **28**, 143 (1979).
[24] T. V. Ramakrishnan and M. Yussouff, Phys. Rev. B **19**, 2775 (1979).
[25] A. D. J. Haymet and D. W. Oxtoby, J. Chem. Phys. **74**, 2559 (1981).
[26] D. W. Oxtoby and A. D. J. Haymet, J. Chem. Phys. **76**, 6262 (1982).
[27] Y. Singh, J. P. Stoessel, and P. G. Wolynes, Phys. Rev. Lett. **54**, 1059 (1985).
[28] W. A. Curtin and N. W. Ashcroft, Phys. Rev. Lett. **56**, 2775 (1986).
[29] K. R. Elder, M. Katakowski, M. Haataja, and M. Grant, Phys. Rev. Lett. **88**, 245701 (2002).
[30] K. R. Elder and M. Grant, Phys. Rev. E **70**, 051605 (2004).
[31] J. Berry, M. Grant, and K. R. Elder, Phys. Rev. E **73**, 031609 (2006).
[32] P. Stefanovic, M. Haataja, and N. Provatas, Phys. Rev. Lett. **96**, 225504 (2006).
[33] K. R. Elder, N. Provatas, J. Berry, P. Stefanovic, and M. Grant, Phys. Rev. B **75**, 064107 (2007).
[34] M. Greenwood, N. Provatas, and J. Rottler, Phys. Rev. Lett. **105**, 045702 (2010).
[35] K. Elder, K. Thornton, and J. Hoyt, Philos. Mag. **91**, 151 (2011).
[36] M. Greenwood, N. Ofori-Opoku, J. Rottler, and N. Provatas, Phys. Rev. B **84**, 064104 (2011).
[37] G. Tegze, L. Gránásy, G. I. Tóth, F. Podmaniczky, A. Jaatinen, T. Ala-Nissila, and T. Pusztai, Phys. Rev. Lett. **103**, 035702 (2009).
[38] K.-A. Wu and P. W. Voorhees, Phys. Rev. B **80**, 125408 (2009).
[39] S. Majaniemi and N. Provatas, Phys. Rev. E **79**, 011607 (2009).
[40] K. R. Elder and Z.-F. Huang, J. Phys.: Cond. Matter **22**, 364103 (2010).
[41] K.-A. Wu, M. Plapp, and P. W. Voorhees, J. Phys.: Cond. Matter **22**, 364102 (2010).
[42] K.-A. Wu, A. Adland, and A. Karma, Phys. Rev. E **81**, 061601 (2010).
[43] K. R. Elder, Z.-F. Huang, and N. Provatas, Phys. Rev. E **81**, 011602 (2010).
[44] M. Greenwood, J. Rottler, and N. Provatas, Phys. Rev. E **83**, 031601 (2011).
[45] K.-A. Wu and P. W. Voorhees, Acta Mater. **60**, 407 (2012).
[46] E. J. Schwalbach, J. A. Warren, K.-A. Wu, and P. W. Voorhees, Phys. Rev. E **88**, 023306 (2013).
[47] S. Alexander and J. McTague, Phys. Rev. Lett. **41**, 702 (1978).
[48] L. Gránásy and T. Pusztai, J. Chem. Phys. **117**, 10121 (2002).
[49] A. R. Denton and N. W. Ashcroft, Phys. Rev. A **39**, 426 (1989).
[50] S. M. Foiles, M. I. Baskes, and M. S. Daw, Phys. Rev. B **33**, 7983 (1986).
[51] S. L. Altmann and A. P. Cracknell, Rev. Mod. Phys. **37**, 19 (1965).
[52] W. R. Fehlner and S. H. Vosko, Can. J. Phys. **54**, 2159 (1976).
[53] F. Podmaniczky, G. I. Tóth, T. Pusztai, and L. Gránásy, J. Cryst. Growth **385**, 148 (2014), the 7th International Workshop on Modeling in Crystal Growth.
[54] K.-A. Wu, C.-H. Wang, J. J. Hoyt, and A. Karma, Phys. Rev. B **91**, 014107 (2015).